The Astrophysical Journal, 672:371–381, 2008 January 1

ABUNDANT CARBON-CHAIN MOLECULES TOWARD THE LOW-MASS PROTOSTAR IRAS 04368+2557 IN L1527

Nami Sakai,[1] Takeshi Sakai,[2] Tomoya Hirota,[3] and Satoshi Yamamoto[1]
Received 2007 June 4; accepted 2007 September 11

ABSTRACT

We have detected the high-excitation lines of carbon-chain molecules such as C_4H_2 ($J = 10_{0,10}$–$9_{0,9}$), C_4H ($N = 9$–8, F_1, F_2), l-C_3H_2 ($4_{1,3}$–$3_{1,2}$), and CH_3CCH ($J = 5$–4, $K = 2$) toward a low-mass star-forming region, L1527. In particular, the F_1 line of C_4H is as strong as 1.7 K (T_{MB}). The rotational temperature of C_4H_2 is determined to be 12.3 ± 0.8 K, which is higher than that in TMC-1 (3.8 K). Furthermore, the column density of C_4H_2 is derived to be about 1/4 of that in TMC-1, indicating that carbon-chain molecules are abundant in L1527 for a star-forming region. Small mapping observations show that the C_4H, C_4H_2, and c-C_3H_2 emissions are distributed from the infalling envelope to the inner part. Furthermore, we have detected the lines of C_5H, HC_7N, and HC_9N in the 20 GHz region. Since the carbon-chain molecules are generally deficient in star-forming cores, the above results cannot simply be explained by the existing chemical models. The following hypothesis is proposed. If the timescale of the prestellar collapse in L1527 were shorter than those of the other star-forming cores, the carbon-chain molecules could survive in the central part of the core. In addition, regeneration processes of the carbon-chain molecules due to star formation activities would play an important role. Evaporation of CH_4 from the grain mantles would drive the regeneration processes. The present observations show new chemistry in a warm and dense region near the protostars, which is named "warm carbon-chain chemistry (WCCC)."

Subject headings: ISM: abundances — ISM: individual (L1527) — ISM: molecules — stars: formation

1. INTRODUCTION

Existence of various carbon-chain molecules is a characteristic feature of the molecular composition in interstellar clouds, and understanding of their production and destruction has been an important target of astrochemistry. Toward this direction, Suzuki et al. (1992) carried out an extensive survey of CCS, HC_3N, HC_5N, and NH_3 toward 49 dense cores. They found that CCS and other carbon-chain molecules represent the early stage of chemical evolution of dense cores, whereas NH_3 represents the advanced stage. A similar result is subsequently obtained for Bok globules by Scappini & Codella (1996). Furthermore, Benson et al. (1998) observed CCS and N_2H^+ toward 60 dense cores and found that the $[N_2H^+]/[CCS]$ ratio is related to the physical evolution of the cores. Ohashi et al. (1999) reported that the distribution of CCS in a starless core of L1544 has a donut-like structure with a scale of 7500 AU. CCS is deficient in the evolved central part, whereas N_2H^+ is centrally concentrated (Tafalla et al. 1998). The chemical model simulation by Aikawa et al. (2001) successfully reproduced such a chemical differentiation, which is mainly caused by the chemical evolutionary effect including depletion of molecules onto dust grains. Now it is generally recognized that CCS and other carbon-chain molecules are abundant in the early stage of chemical evolution and become deficient at the advanced stage.

Recently, we fortuitously detected the high-excitation lines of C_4H_2 ($10_{1,9}$–$9_{1,8}$ and $10_{0,10}$–$9_{0,9}$) toward a low-mass protostar IRAS 04368+2557 in L1527 with the Nobeyama 45 m telescope (NRO 45 m)[4] in the course of the survey observation of complex organic molecules (Sakai et al. 2006, 2007a, 2007b). Although the C_4H_2 lines were detected toward a cold starless core TMC-1, which is a famous carbon-chain rich cloud, and some translucent clouds without star formation activities (e.g., Kawaguchi et al. 1991; Turner et al. 2000), this is the first detection of C_4H_2 toward star-forming regions. More importantly, such high-excitation lines of C_4H_2 have never been detected, even in TMC-1. Detection of a long carbon-chain molecule, C_4H_2, in a dense part of the star-forming region is very surprising in view of the current understanding of the carbon-chain chemistry.

L1527 is a famous dense core in the Taurus molecular cloud with a heavily obscured *IRAS* source (IRAS 04368+2557) located at the center, which is recognized to be a borderline Class 0/Class I object according to André et al. (2000). A molecular bipolar outflow, whose dynamical age is estimated to be 2.0×10^4 yr, is associated with the *IRAS* source (e.g., Tamura et al. 1996). Since the outflow axis is almost in the plane of the sky, the protostellar disk around the central star will have an edge-on geometry. Asymmetric profiles of the H_2CO ($2_{1,2}$–$1_{1,1}$, $3_{1,2}$–$2_{1,1}$) and c-C_3H_2 ($2_{1,2}$–$1_{0,1}$) lines with stronger blueshifted emission than redshifted emission were detected in L1527, suggesting the infall motion (e.g., Zhou et al. 1994; Myers et al. 1995). Ohashi et al. (1997) reported that L1527 may harbor an infalling envelope on the basis of their interferometric observation of $C^{18}O$ ($J = 1$–0), whose radius and mass are estimated to be 2000 AU and 0.04 $M_\odot$, respectively. The dynamical age of the infalling envelope is roughly derived to be 10^5 yr from the accretion rate, which seems to be comparable to the age of the outflow.

Although extensive studies have been performed on physical structure and dynamics of L1527 as mentioned above, little

[1] Department of Physics, University of Tokyo, Hongo, Bunkyo-ku, Tokyo 113-0033, Japan.
[2] Nobeyama Radio Observatory, Minamimaki, Minamisaku, Nagano 384-1305, Japan.
[3] National Astronomical Observatory of Japan, Osawa, Mitaka, Tokyo 181-8588, Japan.

[4] The Nobeyama Radio Observatory is a branch of the National Astronomical Observatory of Japan, National Institutes of Natural Sciences, Japan.

TABLE 1
MOLECULAR LINES OBSERVED TOWARD L1527 ($\Delta\alpha = 0'$, $\Delta\delta = 0'$)

Species	Transition	Frequency (GHz)	T_{MB}[a] (K)	dv[a] (km s^{-1})	$\int T_{MB}\,dv(3\,\sigma)$ (K km s^{-1})	rms[b] (mK)	V_{LSR}[a] (km s^{-1})	Ref.[c]
			L1527					
CCS	$N = 1$–0, $J = 2$–1	22.344033	0.413(13)	0.29(1)	0.131(8)	8.7	5.94	1
$CC^{34}S$	$N = 1$–0, $J = 2$–1	21.930486	...	...	$\leq$0.008	9.6	...	1
c-C_3H_2	$4_{3,2}$–$4_{2,3}$	85.656431	0.584(19)	0.63(2)	0.407(25)	13.2	5.90	2,3
l-C_3H_2	$1_{0,1}$–$0_{0,0}$	20.792588	0.072(11)	0.27(5)	0.021(13)	16.1	5.99	4,5,6
	$2_{1,2}$–$1_{1,1}$	41.198335	0.220(9)	0.56(3)	0.143(21)	12.7	5.85	
	$2_{0,2}$–$1_{0,1}$	41.584676	0.185(11)	0.39(3)	0.078(10)	8.1	5.92	
	$4_{1,3}$–$3_{1,2}$	83.933699	0.403(16)	0.52(2)	0.225(18)	11.3	5.92	
C_4H_2	$5_{1,5}$–$4_{1,4}$	44.471138	0.177(16)	0.66(7)	0.125(22)	11.1	5.88	6,7
	$5_{0,5}$–$4_{0,4}$	44.659015	0.117(17)	0.57(10)	0.078(21)	12.1	5.70	
	$5_{1,4}$–$4_{1,3}$	44.844590	0.211(21)	0.57(7)	0.138(25)	14.7	5.79	
	$9_{0,9}$–$8_{0,8}$	80.383887	0.316(90)	0.33(11)	0.123(63)	64.4	5.76	
	$9_{1,8}$–$8_{1,7}$	80.718829	0.291(68)	0.64(17)	0.206(82)	42.5	5.78	
	$10_{0,10}$–$9_{0,9}$	89.314548	0.126(7)	0.54(4)	0.072(7)	4.6	5.72	
	$10_{1,9}$–$9_{1,8}$	89.687047	0.205(7)	0.66(3)	0.145(10)	5.2	5.82	
	$12_{0,12}$–$11_{0,11}$	107.175007	...	...	$\leq$0.076	46.6	...	
	$12_{1,11}$–$11_{1,10}$	107.622954	0.117(49)	0.54(26)	0.076(70)	42.9	5.94	
C_4H	$N = 9$–8, F_1	85.634004	1.699(20)	0.59(1)	1.069(24)	13.7	5.90	6,8,9
	F_2	85.672579	1.605(19)	0.60(1)	1.047(25)	13.9	5.89	
C_5H	$^2\Pi_{1/2}$, $J = 9/2$–7/2, $F = 5$–4, f	21.480819	0.026(3)	0.42(5)	0.012(2)	1.6	6.03	6,10,11
	$F = 4$–3, f	21.481316	0.020(2)	0.65(8)	0.016(2)	1.5	6.12	
	$F = 5$–4, e	21.484706	0.033(3)	0.39(4)	0.014(2)	1.7	6.01	
	$F = 4$–3, e	21.485258	0.019(3)	0.51(8)	0.011(2)	1.5	5.97	
CH_3CCH	$J = 5$–4, $K = 0$	85.457272	0.946(47)	0.45(3)	0.429(9)	6.3	5.83	6,12,13
	$K = 1$	85.455622	0.890(47)	0.47(3)	0.458(9)	6.2	5.74	
	$K = 2$	85.450730	0.139(53)	0.65(29)	0.088(11)	5.4	5.79	
	$K = 3$	85.442528	...	...	$\leq$0.010	5.3	...	
HC_5N	$J = 7$–6	18.638617	0.343(8)	0.73(2)	0.260(11)	5.1	5.87	6,14,15
HC_7N	$J = 20$–19	22.559907	0.136(13)	0.45(5)	0.066(12)	9.0	5.77	6,16,17
HC_9N	$J = 37$–36	21.498185	0.0092(28)	0.32(12)	0.0032(18)	1.9	5.88	6,17,18
			TMC-1					
C_4H	$N = 9$–8, F_1	85.634004	1.177(210)	0.42(9)	0.558(181)	142	5.71	6,8,9
	F_2	85.672579	0.904(165)	0.65(14)	0.637(230)	117	5.75	
C_5H	$^2\Pi_{1/2}$, $J = 9/2$–7/2, $F = 5$–4, f	21.480819	0.086(6)	0.33(3)	0.032(2)	2.2	5.83	6,10,11
	$F = 4$–3, f	21.481316	0.073(6)	0.31(3)	0.025(2)	2.3	5.93	
	$F = 5$–4, e	21.484706	0.083(6)	0.33(3)	0.032(2)	1.9	5.83	
	$F = 4$–3, e	21.485258	0.071(6)	0.29(3)	0.025(2)	2.0	5.81	
HC_7N	$J = 20$–19	22.559907	1.544(8)	0.41(1)	0.648(4)	3.6	5.73	6,16,17
HC_9N	$J = 37$–36	21.498185	0.171(3)	0.37(1)	0.067(3)	2.1	5.88	6,17,18

NOTES.—Numbers in parentheses represent the errors in units of the last significant digit.
[a] Obtained by the Gaussian fit.
[b] The rms noise averaged over the line width.
[c] References are for the rest frequency, the line strength, the upper- or lower-state energy, the dipole moment, and the rotational constants.
REFERENCES.—(1) Yamamoto et al. 1990; (2) Thaddeus et al. 1985; (3) The Jet Propulsion Laboratory (JPL) Catalog of Line Positions and Intensities; (4) Vrtilek et al. 1990; (5) DeFrees & McLean 1986; (6) The Cologne Database for Molecular Spectroscopy; (7) Killian et al. 1990; (8) Guélin et al. 1982; (9) Wilson & Green 1977; (10) McCarthy et al. 1999; (11) Cernicharo et al. 1987; (12) Burrell et al. 1980; (13) Pracna et al. 1996; (14) Winnewisser et al. 1982; (15) Alexander et al. 1976; (16) Kirby et al. 1980; (17) Bell et al 1997; (18) Iida et al. 1991.

attention has been paid to its chemical composition. Since the detection of C_4H_2 suggests a new aspect of the carbon-chain chemistry, we have further made single dish observations of various carbon-chain molecules toward L1527.

2. OBSERVATIONS

2.1. *Observation with NRO* 45 m

Observations of the molecular lines in the 40 GHz and 80–110 GHz regions (Table 1), except for the lines of CCH, were carried out with NRO 45 m from 2005 to 2007. Survey observations of CCH with NRO 45 m are described in the Appendix. We observed IRAS 04368+2557 in L1527 ($\alpha_{2000.0}, \delta_{2000.0}$) = ($04^h39^m53.89^s$, $26^\circ03'11.0''$) and the cyanopolyyne peak of TMC-1 ($\alpha_{2000.0}$, $\delta_{2000.0}$) = ($04^h41^m42.88^s$, $25^\circ41'27.0''$), unless otherwise noted. The SIS mixer receivers, S40, S80, and S100, were used in the observations, whose typical system temperatures were about 180, 300, and 300 K, respectively. The main-beam efficiency was 0.77 at 43 GHz, while it was 0.51 at 89 GHz. We did not make further corrections of these efficiencies for slightly different frequencies. The beam size of the telescope is $40''$ and $19''$ at 43 and 89 GHz, respectively. The telescope pointing was checked by observing the nearby SiO maser source (NML Tau) every hour. The pointing accuracy was better than $8''$. The position-switching mode was

employed for the observations, where the off position was taken at $\Delta\alpha = 30'$, $\Delta\delta = 30'$. The backend was a bank of acousto-optical radiospectrometers (AOSs). We used eight wide-band AOSs (AOS-W) with individual bandwidths of 250 MHz and eight high-resolution AOSs (AOS-H) with individual bandwidths of 40 MHz. The velocity resolution of AOS-W is 0.84 km s^{-1} at 90 GHz, whereas that of AOS-H is 0.12 km s^{-1}. The intensity scale was calibrated by the chopper wheel method.

2.2. *Observation with Green Bank Telescope*

We observed the spectral lines of some carbon-chain molecules with the Robert C. Byrd Green Bank Telescope (GBT) of the National Radio Astronomy Observatory[5] in 2006 (Sakai et al. 2007c). All the lines in the 20 GHz region listed in Table 1 are observed with GBT. We used the K-band receiver whose instantaneous bandwidth is 4 GHz. The beam size of the telescope is 37″, and the main-beam efficiency is 0.88 at 20 GHz. We did not make further corrections of this efficiency for slightly different frequencies. We observed the center position ($\Delta\alpha = 0'$, $\Delta\delta = 0'$) of L1527 and the cyanopolyyne peak of TMC-1 mentioned above. The pointing of the telescope was checked by observing the nearby continuum sources every hour, and the maximum pointing error was 7″. The frequency-switching mode was employed for the observations. The frequency offset was 3 MHz. The system temperature during the observations ranged from 20 to 50 K. We used the autocorrelators as backends, whose individual bandwidths and resolutions are 50 and 12 kHz, respectively. The resolution corresponds to the velocity resolution of 0.16 km s^{-1}, which is narrower than the typical line width in L1527 (0.5 km s^{-1}). The intensity scale was calibrated by the noise injection. We took the weighted average of the spectra of the right- and left-handed circular polarizations to obtain the final spectrum.

3. RESULT

3.1. *Multitransition Observation of* C_4H_2

As mentioned in § 1, we first detected the two high-excitation lines of C_4H_2, $10_{0,10}$–$9_{0,9}$ (para) and $10_{1,9}$–$9_{1,8}$ (ortho), toward L1527 fortuitously. Their spectral line profiles are shown in Figure 1, and the line parameters derived from the Gaussian fitting procedures are summarized in Table 1. The upper state energies (E_u) of the $10_{0,10}$–$9_{0,9}$ and $10_{1,9}$–$9_{1,8}$ lines, measured from the para and ortho ground states, are 23.6 and 23.2 K, respectively. In spite of the high upper state energy and the high critical density of $\sim 10^6$ cm^{-3}, the observed intensities are as strong as 126 ± 7 and 205 ± 7 mK in T_{MB} for the para and ortho lines, respectively. Such high-excitation lines of C_4H_2 have not been detected in TMC-1. The highest transitions reported for TMC-1 are $8_{0,8}$–$7_{0,7}$ and $8_{1,8}$–$7_{1,7}$ in the 70 GHz region, whose intensities are 56.3 and 122.1 mK, respectively (Turner et al. 2000). The intensities of the $10_{0,10}$–$9_{0,9}$ and $10_{1,9}$–$9_{1,8}$ lines toward TMC-1 are expected to be lower than those toward L1527 by more than an order of magnitude, according to the extrapolation from the existing observational data (Kawaguch et al. 1991; Turner et al. 2000; Kaifu et al. 2004). The line width of C_4H_2 is 0.54 ± 0.03 km s^{-1} for $10_{0,10}$–$9_{0,9}$ and 0.66 ± 0.04 km s^{-1} for $10_{1,9}$–$9_{1,8}$, and no significant velocity shift is seen from the systemic velocity ($\sim$5.85 km s^{-1}) of the L1527 core (e.g., Zhou et al. 1994; Hirota et al. 2001). Therefore, these high-excitation lines would be emitted from the dense inner part of the L1527 core, not from the rather diffuse foreground and background gas.

In order to investigate the excitation condition of the C_4H_2 lines in L1527, we further observed the other transitions of C_4H_2 with NRO 45 m (Table 1). The rotational diagram of the ortho species for L1527 is shown in Figure 2. The corresponding rotational diagram for TMC-1 is also shown. We determined the rotational temperature and the column density of C_4H_2 assuming the LTE condition, where we take the effect of the optical depth into account as

$$T_{MB} = [B_\nu(T_{ex}) - B_\nu(T_b)](1 - e^{-\tau}), \quad (1)$$

where $B_\nu(T)$ is the Planck function and T_b is the temperature of the cosmic background radiation. The optical depth, τ, is represented as

$$\tau = \left(c^2/8\pi\nu^2\right) N_u A_{ul} e^{h\nu/kT_{ex}} \left(1 - e^{-h\nu/kT_{ex}}\right) (4 \ln 2/\pi)^{1/2} (1/\Delta\nu), \quad (2)$$

and

$$N_u = N g_u e^{-E_u/kT_{ex}} / U(T_{ex}), \quad (3)$$

where A_{ul} is the Einstein A-coefficient of the transition between the states u and l, N is the column density in the line of sight, g_u is the degeneracy of the upper state, E_u is the upper state energy, and $U(T_{ex})$ is the partition function. By the least-squares analysis, the column density and T_{ex} were determined. The ortho and para lines were analyzed separately.

The rotational temperature and the column density of the ortho species in L1527 averaged over the telescope beam and along the line of sight are derived to be 12.3 ± 0.8 K and (1.18 ± 0.05) × 10^{12} cm^{-2}, respectively. The highest optical depth of the C_4H_2 lines is 0.03 for the $9_{1,8}$–$8_{1,7}$ line. The rotational temperature of C_4H_2 in TMC-1 is similarly evaluated to be 3.8 ± 0.5 K from the data by Kaifu et al. (2004) and Turner et al. (2000), where the highest optical depth is 0.59 for the $4_{1,3}$–$3_{1,2}$ line. Thus, the rotational temperature in L1527 is higher than that in TMC-1. For the para species, the rotational temperature is assumed to be the same as that of the ortho species, and the column density is derived to be (0.40 ± 0.05) × 10^{12} cm^{-2}. The total column density in L1527 is (1.6 ± 0.1) × 10^{12} cm^{-2}, which is about a quarter of that in TMC-1 ([7.1 ± 2.6] × 10^{12} cm^{-2}). The ortho-to-para ratio is evaluated to be 3.0 ± 0.4 and 3.6 ± 1.6 for L1527 and TMC-1, respectively, which is consistent with the statistical value of 3.

3.2. *High-Excitation Lines of Carbon-Chain Molecules*

In addition to C_4H_2, we detected the high-excitation lines of C_4H ($N = 9$–8, F_1 and F_2, $E_u = 20.5$ and 20.6 K, respectively), l-C_3H_2 ($4_{1,3}$–$3_{1,2}$, $E_u = 23.4$ K), c-C_3H_2 ($4_{3,2}$–$4_{2,3}$, $E_u = 29.1$ K), and CH_3CCH ($J = 5$–4, $K = 2$, $E_u = 41.1$ K). The line parameters are summarized in Table 1, and the line profiles except for C_4H are shown in Figure 1. The profile of C_4H ($N = 9$–8, F_2) is referred to in the center position of Figure 3. The intensities of the F_1 and F_2 lines of C_4H are as strong as 1.7 and 1.6 K, respectively, in T_{MB}, being stronger than those in TMC-1 (1.2 and 0.9 K, respectively). These results indicate that various carbon-chain molecules, C_nH_m, exist in the dense part of the L1527 core, as in the case of C_4H_2.

We can estimate the gas kinetic temperature of that part using the $K = 1$ and 2 lines of CH_3CCH. Although the $K = 1$ and 2 states belong to the same symmetry species (para), the radiative

[5] The National Radio Astronomy Observatory is a facility of the National Science Foundation operated under cooperative agreement by Associated Universities, Inc.

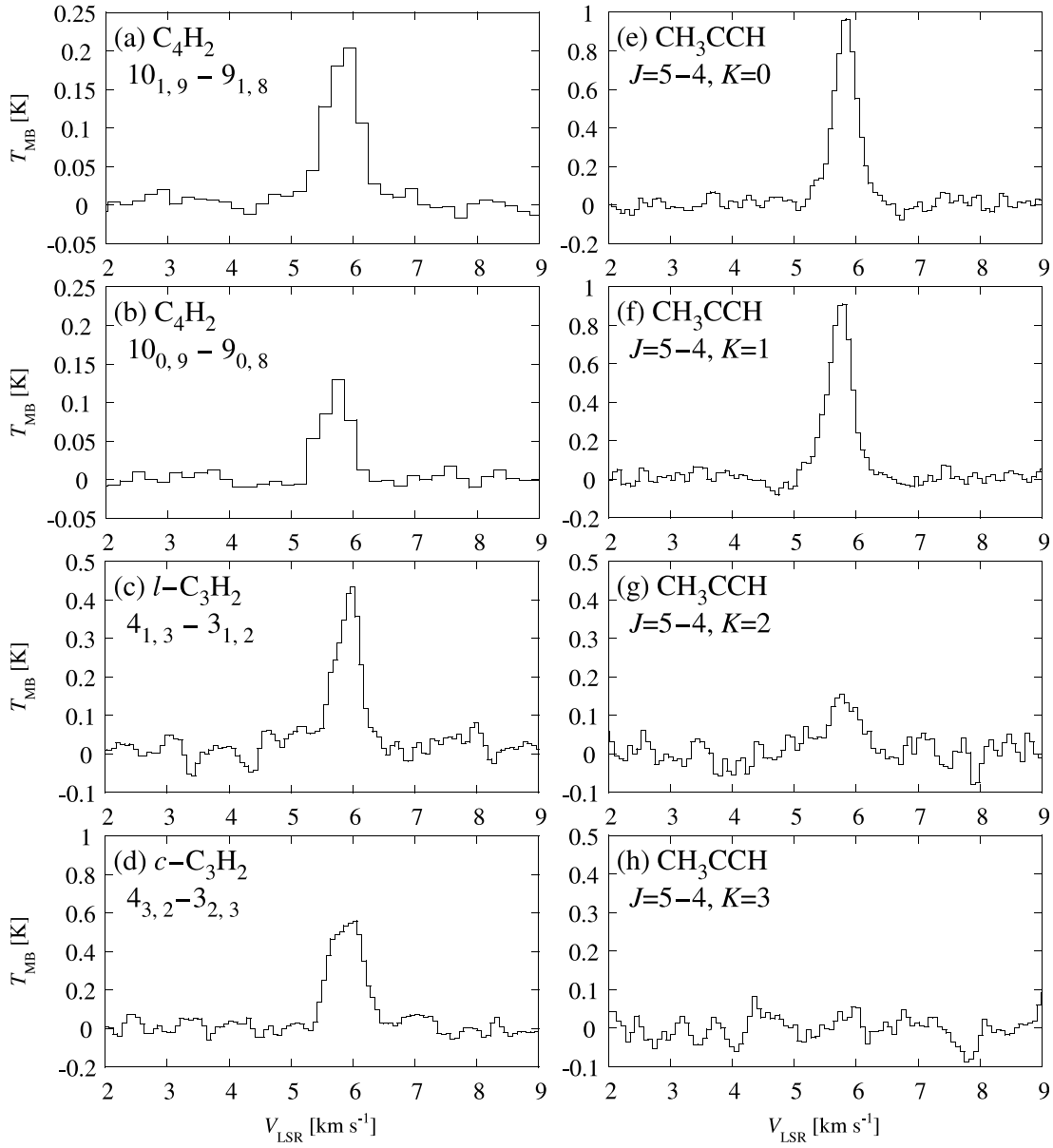

FIG. 1.—Spectral line profiles observed toward L1527.

interconversion between them is very slow. Therefore, these two states are readily thermalized to the gas kinetic temperature by collision with the H_2 molecules, as in the case of the NH_3 $(J, K) = (1, 1)$ and $(2, 2)$ lines. From the integrated intensities of the $K = 1$ and 2 lines, we derive the gas kinetic temperature to be 13.9 K. This is the effective temperature averaged over the telescope beam and along the line of sight. With this temperature, the integrated intensity of the $K = 3$ line is estimated to be 0.005 K km s^{-1}. This is consistent with the upper limit (3 σ) given in Table 1. The total column density of CH_3CCH is determined to be 6.0×10^{13} cm^{-2}, assuming the LTE condition with the rotational temperature of 13.9 K.

In TMC-1, the rotational temperature of various carbon-chain molecules ranges mostly from 4 to 8 K, which is lower than the gas kinetic temperature of 10 K (e.g., Kawaguchi et al. 1991; Kalenskii et al. 2004; Takano et al. 1990). This means that the density of the emitting region is not high enough to thermalize the rotational level population to the gas kinetic temperature for most cases. On the other hand, the rotational temperature of C_4H_2 is 12.3 K in L1527 and is close to the gas kinetic temperature of 13.9 K. This means that the density of the emitting region of carbon-chain molecules in L1527 is higher than the critical density of the C_4H_2 lines (typically 10^6 cm^{-3}). Therefore, the high-excitation lines do not originate from the foreground or background gas of L1527, but from the inner dense part around the protostar.

3.3. *Profile Maps of* C_4H *and* HCO^+

Figure 3 shows the profile map of the C_4H ($N = 9$–$8, F_2$) line around the protostar observed with NRO 45 m. The grid spacing is 18.7″, which corresponds to the beam size of NRO 45 m at 89.3 GHz. The line parameters are summarized in Table 2. In all the spectra except for the southeast position ($\Delta\alpha = 18.7''$, $\Delta\delta = -18.7''$), no velocity shift is seen from the systemic velocity of the L1527 core. The V_{LSR} value of the southeast position is 5.96 km s^{-1}, which is slightly higher than those in other positions. According to the HCN ($J = 1$–0) map by Choi et al. (1999) and the $C^{18}O$ ($J = 2$–1) map by Zhou et al. (1994), there exists a small extension to the southeast direction, which would be another core.

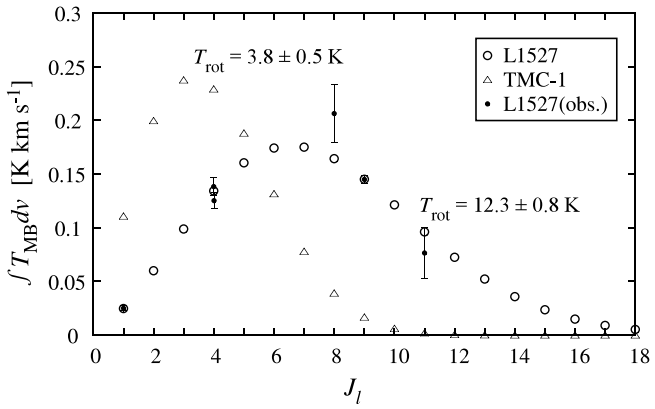

FIG. 2.—Rotational diagram of the ortho-C_4H_2. The filled circles represent the observed integrated intensities in L1527, whereas the open circles represent the best-fit values. The open triangles denote the best-fit values for TMC-1, where the observation data are taken from Turner et al. (2000) and Kaifu et al. (2004).

The interferometric observation of $C^{18}O$ ($J = 1$–0) by Ohashi et al. (1997) shows that an infalling envelope with the edge-on geometry extends toward the north–south direction. The north–south extension of the C_4H distribution is consistent with the size of the infalling envelope (~25″), whereas the east–west extension of the distribution seems to be larger than the corresponding size of the infalling envelope (~10″). Although the C_4H emission is extended over the 40″ scale, the integrated intensity is the highest toward the center. This indicates that a large amount of C_4H exists even in the vicinity of the protostar in L1527. More importantly, the line width toward the center is significantly broader than those toward surrounding positions. The line width is consistent with the infalling envelope pointed out by Ohashi et al. (1997); the broadening is due to the combination effect of the rotational and infalling motions. Hence, C_4H is distributed continuously from the infalling envelope (~5600 AU) to the inner part. Similar features are also seen in the profile maps of the C_4H ($N = 9$–8, F_1) line, the $C_4H_2(10_{1,9}$–$9_{1,8})$ line, and the high-excitation line of c-$C_3H_2(4_{3,2}$–$4_{2,3})$ (Table 2). The broadening of the c-$C_3H_2(2_{1,2}$–$1_{0,1})$ line toward the center position was also pointed out by Myers et al. (1995). They interpreted this as an infalling signature.

Figure 4 shows the profile map of the HCO^+ ($J = 1$–0) line. Only five positions around the protostar are observed. In this profile map, the wing components due to the outflow extending toward the east–west direction can be seen in the velocity range from 1 to 10 km s^{-1}. In addition, the infall signature can also be recognized in absorption at V_{LSR} of 6 km s^{-1} owing to the high optical depth of the HCO^+ line. These profiles are consistent with the previous results (e.g., Tamura et al. 1996; Hogerheijde et al. 1998). The line profiles of the C_4H, C_4H_2, and c-C_3H_2 lines do not show the wing profile seen in the HCO^+ spectra, further confirming that the high-excitation lines

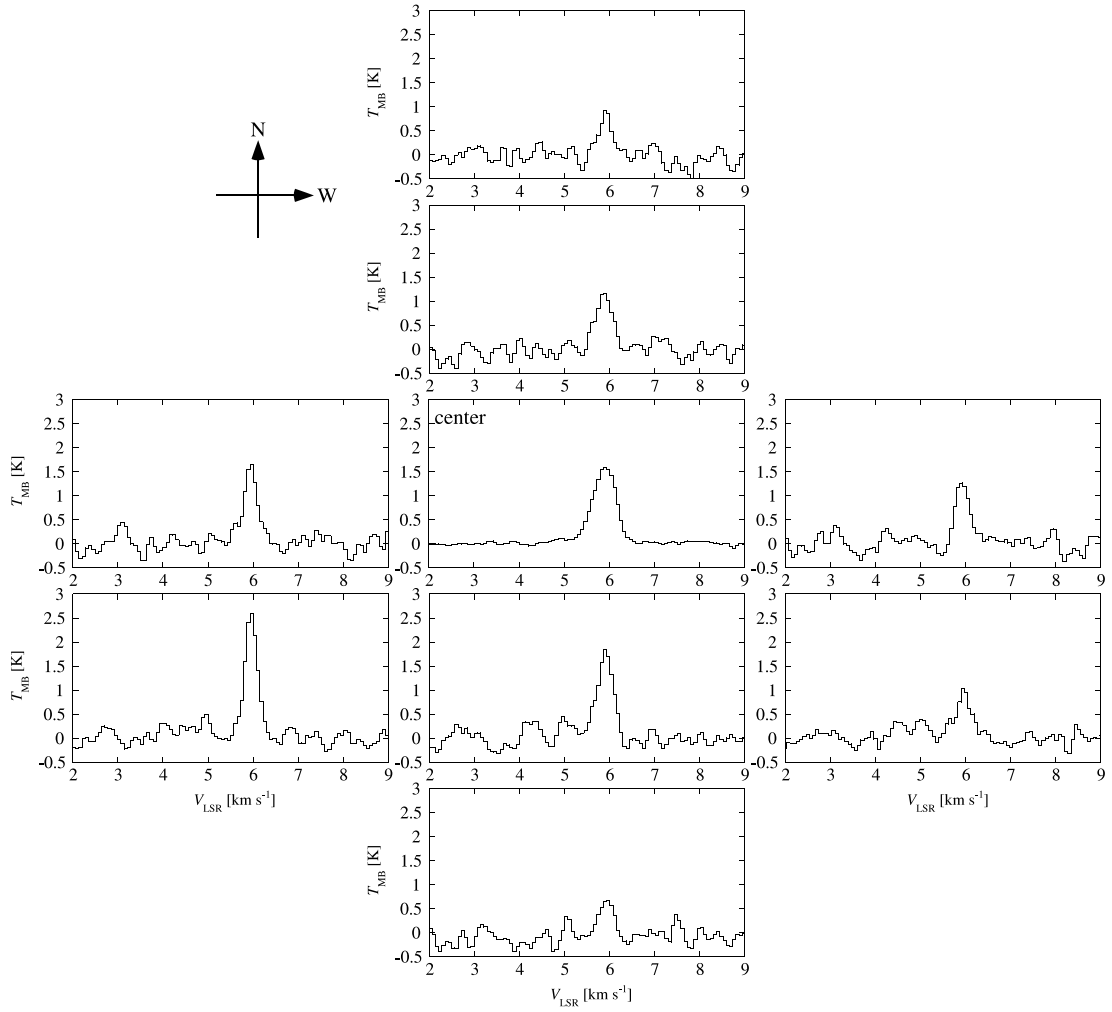

FIG. 3.—Profile map of C_4H ($N = 9$–8, F_2) observed toward L1527. Grid spacing is 18.7″. The center position is toward IRAS 04368+2557.

TABLE 2
LINE PARAMETERS OBSERVED AROUND THE PROTOSTAR IN L1527

Species	Transition	Position ($\Delta\alpha$, $\Delta\delta$) (arcsec)	T_{MB} (K)	dv (km s^{-1})	$\int T_{MB}\,dv$ (3 σ) (K km s^{-1})	rms (mK)	V_{LSR} (km s^{-1})
C_4H.....	$N = 9-8$, F_1	(0, +37.4)	0.64(10)	0.33(6)	0.22(7)	72	5.90
		(0, +18.7)	1.02(8)	0.46(4)	0.49(7)	53	5.91
		(+18.7, 0)	1.60(8)	0.40(3)	0.65(7)	58	5.94
		(−18.7, 0)	1.16(8)	0.42(4)	0.52(7)	57	5.88
		(+18.7, −18.7)	2.35(10)	0.37(2)	0.87(7)	64	6.00
		(0, −18.7)	1.79(9)	0.40(2)	0.75(7)	59	5.91
		(−18.7, −18.7)	0.99(10)	0.31(4)	0.32(6)	70	5.91
		(0, −37.8)	0.53(11)	0.29(7)	0.15(7)	77	5.98
	$N = 9-8$, F_2	(0, +37.4)	0.87(11)	0.33(5)	0.31(7)	71	5.91
		(0, +18.7)	1.15(9)	0.43(4)	0.52(8)	62	5.88
		(+18.7, 0)	1.56(10)	0.37(3)	0.64(8)	73	5.95
		(−18.7, 0)	1.31(10)	0.35(3)	0.50(8)	76	5.93
		(+18.7, −18.7)	2.57(10)	0.33(1)	0.93(7)	68	5.96
		(0, −18.7)	1.78(9)	0.41(2)	0.79(8)	64	5.90
		(−18.7, −18.7)	0.90(8)	0.44(4)	0.41(7)	56	5.92
		(0, −37.8)	0.71(10)	0.32(5)	0.24(8)	78	5.93
C_4H_2.....	$10_{1,9}-9_{1,8}$	(0, +18.7)	0.14(3)	0.55(15)	0.08(4)	24	5.66
		(+18.7, 0)	0.11(3)	0.56(19)	0.07(4)	23	5.82
		(−18.7, 0)	0.14(4)	0.58(17)	0.09(5)	26	5.89
		(0, −18.7)	0.18(3)	0.52(11)	0.11(4)	23	5.81
c-C_3H_2.....	$4_{3,2}-4_{2,3}$	(0, +37.4)	0.39(19)	0.12(8)	0.05(4)	116	5.88
		(0, +18.7)	0.64(10)	0.35(6)	0.24(8)	73	5.89
		(+18.7, 0)	...	...	$\leq$0.06	92	...
		(−18.7, 0)	0.42(13)	0.21(7)	0.09(5)	89	5.89
		(+18.7, −18.7)	0.60(13)	0.19(5)	0.13(5)	91	5.90
		(0, −18.7)	0.58(10)	0.35(7)	0.21(7)	69	5.96
		(−18.7, −18.7)	0.41(14)	0.15(6)	0.07(4)	101	5.91
		(0, −37.8)	0.24(15)	0.16(11)	0.04(5)	106	5.84

NOTE.—See Table 1 for the (0, 0) position.

of the various carbon-chain molecules do not come from the outflowing material.

3.4. *Long Carbon-Chain Molecules*

In the GBT observation, we have detected the spectral lines of some long carbon-chain molecules, C_5H, HC_5N, HC_7N, and HC_9N, a part of which are shown in Figure 5. We have also detected the lines of C_6H, C_6H_2, and C_6H^-, as reported in a separate paper (Sakai et al. 2007d). In interstellar clouds, C_6H has so far been detected in TMC-1 and the Horsehead nebula (Suzuki et al. 1986; Teyssier et al. 2004), C_6H_2 has been detected only in TMC-1 (Langer et al. 1997), and C_5H has been detected in

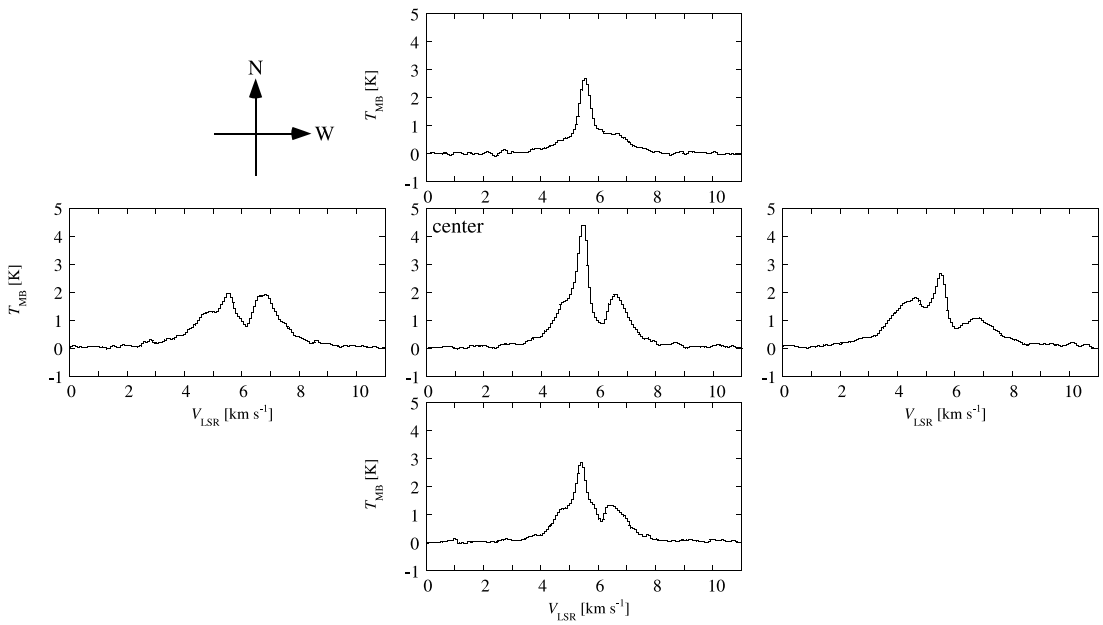

FIG. 4.—Profile map of HCO^+ ($J = 1-0$) observed toward L1527. Grid spacing is 18.7″. The center position is toward IRAS 04368+2557.

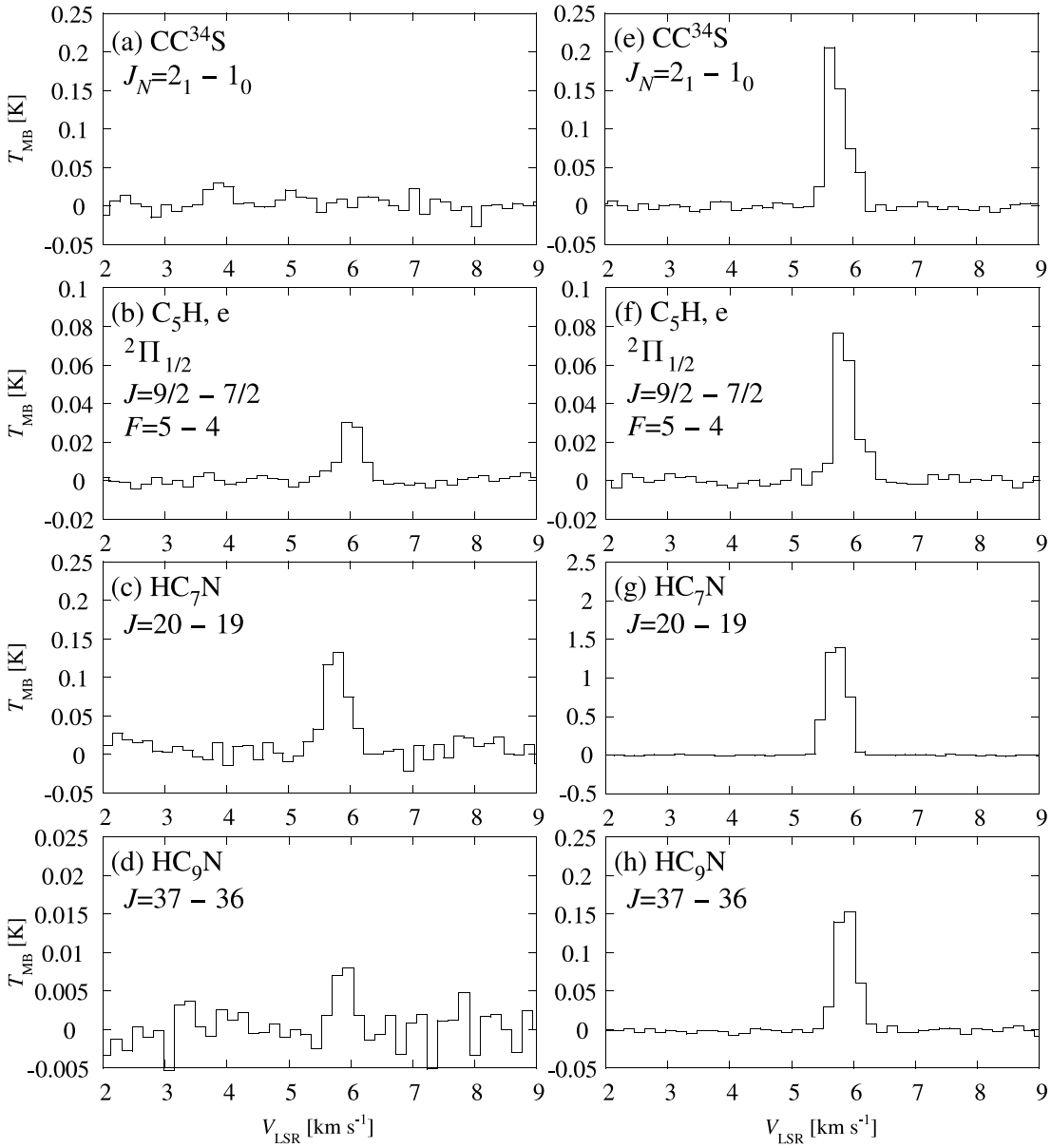

FIG. 5.—Spectral line profiles observed toward L1527 (*left*) and TMC-1 (*right*).

TMC-1 and a translucent cloud, CB 17 (Cernicharo et al. 1987; Turner et al. 2000). Although the detection of HC_7N in Sgr B2 is claimed by Turner (1989), it still remains uncertain. The detection of these carbon-chain molecules except for HC_5N in a star-forming region is therefore surprising by itself, although these are not high-excitation lines. Thus, it is further confirmed that L1527 is a unique star-forming region harboring various carbon-chain molecules. For comparison, we present the spectra of these molecules taken toward TMC-1 and the spectra of $CC^{34}S$ toward the both sources. The intensities of the C_5H and C_6H lines in L1527 are 1/3 and 1/6 of those in TMC-1, respectively (see Sakai et al. [2007d] for the C_6H data). On the other hand, $CC^{34}S$ is weaker in L1527 than TMC-1 by a factor of 10, which is consistent with the result by Hirota et al. (2001). Similarly, the HC_5N, HC_7N, and HC_9N lines are weaker in L1527 than in TMC-1 (see Kaifu et al. [2004] for the HC_5N data in TMC-1).

3.5. *Column Densities of Carbon-Chain Molecules*

The column densities of l-C_3H_2, C_4H, C_5H, HC_5N, HC_7N, and HC_9N in L1527 are derived under the assumption of the LTE condition, where the effect of the optical depth is taken into account. Only one rotational line was observed for each molecule, and hence, the excitation temperature is assumed to be 12.3 K. The column densities of C_4H, C_5H, HC_7N, and HC_9N in TMC-1 are also derived in a manner similar to the L1527 case , where the excitation temperatures are assumed to be 6.7 K for C_4H and C_5H, 7.7 K for HC_7N, and 8.4 K for HC_9N. The excitation temperatures of C_4H and C_5H are assumed to be the same as that of C_6H (Sakai et al. 2007d), whereas those of HC_7N and HC_9N are taken from Kalenskii et al. (2004). The optical depths of the C_4H($N = 9–8$, F_1 and F_2) lines are 0.21 and 0.19 for L1527, and 0.44 and 0.25 for TMC-1, respectively, whereas those of the other lines are much less than 1. As for C_5H in TMC-1, the change in T_{ex} by 1 K causes the change in the derived column density by less than 3%. As for C_4H in TMC-1, the column density is 2.0×10^{14} cm^{-2} and 4.9×10^{14} cm^{-2} for T_{ex} of 7.7 K and 5.7 K, respectively, because the optical depth becomes higher for the lower T_{ex} assumed. The results are summarized in Table 3, along with the column densities of a few molecules in TMC-1 taken from the literature.

TABLE 3
Column Densities of Various Carbon-Chain Molecules

Species	N_{L1527} (cm^{-2})	N_{TMC-1} (cm^{-2})
CH_3CCH	6.0×10^{13}	6×10^{13}[a]
l-C_3H_2	1.1×10^{12}	2.5×10^{12}[b]
C_4H_2	1.6×10^{12}	7.1×10^{12}
C_6H_2	1.5×10^{11}[c]	1.8×10^{11}[c]
C_4H	1.9×10^{14}	2.9×10^{14}
C_5H	8.9×10^{11}	1.7×10^{12}
C_6H	6.2×10^{11}[c]	3.0×10^{12}[c]
HC_5N	5.4×10^{12}	6.3×10^{13}[d]
HC_7N	1.5×10^{12}	2.3×10^{13}
HC_9N	1.4×10^{11}	4.8×10^{12}
CCS	5.1×10^{12}[e]	6.6×10^{13}[e]

[a] Value from Irvine et al. 1981.
[b] Value from Cernicharo et al. 1991.
[c] Value from Sakai et al. 2007c.
[d] Value from Takano et al. 1990.
[e] Value from Hirota et al. 2001.

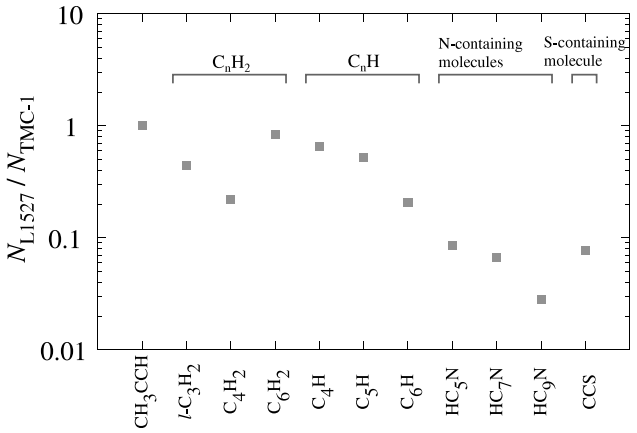

Fig. 6.—Column density ratios between TMC-1 and L1527, N_{L1527}/N_{TMC-1}, for various carbon-chain molecules.

Figure 6 shows the ratios of the column densities between L1527 and TMC-1 for various carbon-chain molecules. The ratio significantly varies from species to species, indicating that the chemical composition of L1527 is not a copy of that of TMC-1. In L1527, the carbon-chain molecules, C_nH_m, are as abundant as in TMC-1, but the N- and S-containing carbon-chain molecules are rather deficient. Furthermore, the ratio tends to decrease for longer chains. These results suggest new carbon-chain chemistry in L1527.

4. DISCUSSION

4.1. *Comparison with Other Sources*

It has been recognized that the carbon-chain molecules are generally deficient in low-mass star-forming regions (e.g., Suzuki et al. 1992). Actually, the $10_{0,10}-9_{0,9}$ and $10_{1,9}-9_{1,8}$ lines of C_4H_2 were not detected in our previous observation toward NGC 1333 IRAS 4B by using NRO 45 m, although the rms noise level achieved is as low as 3.6 mK in T_{MB} (Sakai et al. 2006). Carbon-chain molecules, C_nH_m ($n \geq 3$), are hardly detected in the line surveys of the low-mass star-forming region IRAS 16293−2422 (van Dishoeck et al. 1995; Castets et al. 2005). Although the CH_3CCH lines are detected toward IRAS 16293−2422, its intensities are weaker than that in L1527. Instead, various saturated complex organic molecules like $HCOOCH_3$ and $(CH_3)_2O$ are detected in these two representative low-mass star-forming regions. Such a hot-core-like chemical composition is now recognized as the hot corino chemistry, where the rotational temperatures of the complex organic molecules are typically 40–100 K (e.g., Cazaux et al. 2003; Bottinelli et al. 2004). In contrast, complex organic molecules were not detected in L1527 even by a very sensitive observation with NRO 45 m (Sakai et al. 2007b). This means that the chemical composition is different among the low-mass Class 0 protostars. Such differences would possibly reflect some differences in star formation processes and/or initial physical conditions.

Alternatively, there might be a possibility that the difference originates from that in initial elemental abundances; namely, L1527 is in the C-rich condition. However, the fractional abundances of H_2CO is comparable to that in the other Class 0 sources like NGC 1333 IRAS 4A/B (e.g., Maret et al. 2004). The CH_3OH and SO lines are also observed toward L1527 by Takakuwa et al. (2000) and in our preliminary line survey, respectively. It is therefore difficult to explain the existence of various carbon-chain molecules by the difference in initial elemental abundances.

4.2. *Timescale of the Prestellar Collapse*

A current explanation on the deficiency of carbon-chain molecules in the central part of the core is the gas-phase destruction and the depletion onto dust grains. Both processes would have a timescale of 10^5 yr for the H_2 density of 10^5 cm^{-3}, which is approximately comparable to the dynamical timescale of the core. If the prestellar collapse of L1527 were close to the freefall case and were faster than those in other star-forming cores, chemical evolution would not be able to follow it. In the result, carbon-chain molecules could survive, even in the central part of the core. Although no other direct evidence of such a fast collapse has been reported, this hypothesis would possibly account for the continuous distribution of the carbon-chain molecule emissions from the infalling envelope to the inner part. However, the situation may be more complicated, because the chemical composition of L1527 is not a copy of that of TMC-1. The abundances of CCS, HC_5N, HC_7N, and HC_9N are lower in L1527 than in TMC-1; the C_nH_m species seem to be exceptionally abundant among various series of the carbon-chain molecules. This implies that the C_nH_m species have a longer lifetime than the other series of carbon-chain molecules. Alternatively, the C_nH_m species are selectively regenerated near the protostar. The latter possibility is discussed in § 4.3.

Even if the C_nH_m species have a longer lifetime, they will be destroyed or depleted eventually in the innermost part near the protostar. Then their distribution would have a small hole around the protostar. According to the model of the infalling envelope of L1527 by Ohashi et al. (1997), the line width of 0.6 km s^{-1} observed for C_4H corresponds to the diameter of ~800 AU around the protostar. Therefore, C_4H and other carbon-chain molecules may be destroyed approximately inside this diameter, and such a hole structure with the apparent size of a few arcseconds may be detected by a high spatial resolution observation. A critical comparison of the observed distribution with the chemical model simulation of a dynamically contracting cloud will be very interesting in order to confirm the fast collapse scenario.

4.3. *Regeneration of Carbon-Chain Molecules*

As mentioned above, some carbon-chain molecules may be regenerated in the vicinity of the protostar. In fact, we have noticed additional evidence of the regeneration of CCH (Fig. 7). Figure 7 shows a plot of the column densities of CCH and $HN^{13}C$. The derivation of the CCH column densities is described in the

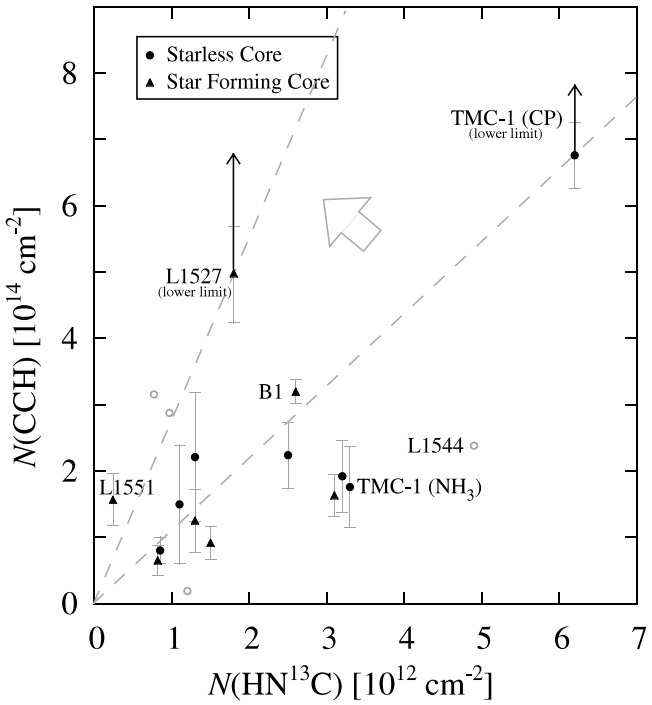

FIG. 7.—Plot of the column densities of CCH and $HN^{13}C$. Open circles represent the data which are derived by assuming the excitation temperature given in Table 4.

Appendix, and the $HN^{13}C$ data are taken from Hirota et al. (1998). We choose $HN^{13}C$ as a standard tracer of the dense gas, whose $J = 1–0$ line is simultaneously observed with the CCH lines. Since the $HN^{13}C$ abundance shows little chemical evolutionary effect, $HN^{13}C$ can be used as a standard molecule (Hirota et al. 1998). As seen in Figure 7, CCH is more abundant toward the cyanopolyyne peak (CP) than toward the ammonia peak (NH_3) in the TMC-1 ridge, the latter being evolved. Furthermore, the CCH column density at the TMC-1 (NH_3) is almost comparable to that toward an evolved starless core like L1544. In contrast, Figure 7 clearly shows that CCH is exceptionally abundant in L1527. Moreover, the [CCH]/[$HN^{13}C$] ratio is higher than those of other starless and star-forming cores, indicating that the CCH abundance in the dense part of the core is enhanced in L1527 in comparison with other starless cores and star-forming regions. Note that the CCH column densities in TMC-1 and L1527 are lower limits, because of the high optical depth, as mentioned in the Appendix. However, it is further confirmed that the column density of CCH in L1527 is higher than that of TMC-1, according to our observations of $C^{13}CH$ in both sources (N. Sakai et al., in preparation).

This cannot be explained simply by adjusting the timescale of the prestellar collapse, but seems to require some regeneration mechanisms in the vicinity of the protostar. One possibility is the evaporation of CH_4 from the grain mantles due to protostellar activities. CH_4 is known to be an important constituent in the H_2O ice, whose abundance is $\sim 3.5\%$ of the H_2O ice according to the *Spitzer* observations (K. Öberg et al. 2007, private communication), although L1527 itself is not observed. It has relatively low sublimation temperature ($\sim$30 K) in comparison with those of CH_3OH and H_2CO ($\sim$100 K). If CH_4 is well accumulated in the grain mantles during the cold prestellar phase, its evaporation would be an important supply of hydrocarbons, which causes the subsequent carbon-chain production in the gas phase.

It should be noted that the gas kinetic temperature as well as the rotational temperature of C_4H_2 obtained in the previous sections are the effective temperatures averaged over the telescope beam and along the line of sight. Since the lower excitation lines are usually more extended than the higher excitation lines, the derived temperature tends to be lower than that of the central part near the protostar. Therefore, the temperature would be higher than 30 K, at least near the protostar, and CH_4 can be evaporated from dust grains there. According to a radiation hydrodynamic model of protostellar collapse by Masunaga & Inutsuka (2000), the diameter of the region where the temperature is higher than 30 K is about 2000 AU for a 1 $M_\odot$ cloud, and the corresponding size for the temperature of 100 K is about 200 AU, although these sizes depend on the mass of the protostar formed, the structure of the protostellar disk, and so on. Therefore, the warm region where CH_4 is evaporated can substantially be larger than hot cores or hot corinos.

This is new carbon-chain chemistry in a warm and dense region, and we call this "warm carbon-chain chemistry (WCCC)." We use the term "warm," because the gas kinetic temperature is not as high as that in hot cores and hot corinos. In WCCC, CCS can remain deficient if sulfur is still depleted on dust grains. Furthermore, the formation of HC_nN is slower than that of C_nH_m (e.g., Turner et al. 1998), which makes the abundances of HC_nN relatively low. Longer chains also tend to be produced more slowly than shorter chains. The chemistry of protostellar cores including WCCC is carefully modeled in a recent paper by Aikawa et al. (2007). They successfully demonstrate that the carbon-chain molecules, C_nH_m, are certainly regenerated in the vicinity of the protostar. If the regeneration processes are taking place for the C_nH_m molecules, their distribution would be concentrated around the protostar. Therefore, the high-resolution observation will allow us to investigate the contribution of the regeneration process by comparing the result with the chemical model calculation.

However, we must realize that such regeneration of the carbon-chain molecules due to WCCC has not been found in other representative low-mass star-forming regions like NGC 1333 IRAS 4B (Sakai et al. 2006) and IRAS 16293−2422 (van Dishoeck et al. 1995). The necessary condition for WCCC may therefore be related to the fast collapse scenario. As shown in Figure 7, the [CCH]/[$HN^{13}C$] ratio is slightly higher in the star-forming cores, B1 and L1551, than the other sources except for L1527. In these star-forming cores, the regeneration process may also have taken place to some extent. Furthermore, IRAS 16293−2422 and NGC 1333 IRAS 4B are parts of active cluster-forming regions, while L1527 is a rather simple region. It therefore seems important to consider the environmental effect. Sensitive observations of carbon-chain molecules toward various star-forming regions would be needed for understanding the necessary condition for WCCC.

5. SUMMARY

1. We detected the high-excitation lines of c-C_3H_2, l-C_3H_2, C_4H_2, C_4H, and CH_3CCH in L1527. Particularly, the line intensities of C_4H are as strong as 1.6–1.7 K. The rotational temperature of C_4H_2 is determined to be 12.3 K. This is close to the gas kinetic temperature (13.9 K) derived from the intensity ratio of the $K = 1$ and 2 lines of CH_3CCH. Therefore, the emissions of the carbon-chain molecules come from the warm and dense part of the protostellar core.

2. The distribution of C_4H is extended over the 40″ scale including the infalling envelope traced by $C^{18}O$ ($J = 1–0$). The line width toward the center is broader than those toward the surrounding positions. This indicates that the C_4H emission is continuously

distributed from the infalling envelope to the inner part. The distributions of c-C_3H_2 and C_4H_2 are essentially the same as that of C_4H.

3. We also detected the lines of some long carbon-chain molecules, C_5H, HC_5N, HC_7N, and HC_9N. This is the first detection of C_5H, HC_7N, and HC_9N toward star-forming regions. In L1527, the C_nH_m species are as abundant as in TMC-1, but N- and S-containing carbon-chain molecules are rather deficient.

4. One possible explanation of the high abundances of the carbon-chain molecules in L1527 would be a shorter collapse time of the prestellar core than in the other star-forming regions, which is close to the freefall time. In this case, some kind of carbon-chain molecules may survive even in the central part of the core.

5. The regeneration processes of C_nH_m would also play an important role. Such regeneration would start from the evaporation of CH_4 in the vicinity of the protostar (warm carbon-chain chemistry [WCCC]). However, an additional condition is needed for WCCC, considering that WCCC is not seen in IRAS 16293−2422 and NGC 1333 IRAS 4B. This condition may be related to the difference in the timescale of the prestellar collapse.

The authors thank Yuri Aikawa, Eric Herbst, Ewine van Dishoeck, Jose Cernicharo, Nagayoshi Ohashi, and Shuichiro Inuzuka for their valuable comments and Karin Öberg for providing us the information on the CH_4 ice. This study is supported by Grants-in-Aid from the Ministry of Education, Culture, Sports, Science, and Technologies (14204013, 15071201, and 19-6825).

APPENDIX

A SURVEY OF CCH IN DARK CLOUD CORES

We conducted a survey observation of CCH ($N = 1$–0) toward various low-mass starless cores and star-forming regions with NRO 45 m in 1992. The observed sources are listed in Table 4. The beam efficiency was 0.55 in 1992. The position-switching mode was employed, where the off position was taken at $\Delta\alpha = 10'$, $\Delta\delta = 0'$. The other observational details are described in § 2.1. The CCH lines were detected in all the sources observed.

The $N = 1$–0 transition of CCH consists of six fine and hyperfine structure components. A simultaneous fit on the intensities of these components is carried out to determine the total optical depth and the excitation temperature of CCH, from which the column density of CCH is evaluated under the assumption of LTE. For TMC-1 (CP), TMC-1C, L1495B, and L1544, all the components except for the two weakest components are optically thick. In L1527, the self-absorption dips are observed, and even the weakest hyperfine component would be optically thick. We derive the optical depth of the weakest hyperfine components assuming the excitation temperature of 12.3 K for L1527, which is assumed to be the same as that obtained for C_4H_2 in this study, and 6.7 K for TMC-1 (CP), which is taken from that of C_6H reported by Sakai et al. (2007d). We employed the excitation temperature of C_6H rather than that of C_4H_2 (3.8 K), because we cannot derive the column density in the latter case. Because of these reasons the derived column densities for L1527 and TMC-1 seem to be lower limits. For L1495B, TMC-1C, and L1544, we assume the excitation temperature of 4.3 K as a typical value of that for other starless cores. For L183, only the strongest hyperfine component is detected, and hence, its optical depth is derived by assuming the excitation temperature of 4.3 K. Table 4 shows the excitation temperatures, the column densities and the optical depths of CCH. The excitation temperatures range from 4.0 to 9.4 K, but are distributed around 4.3 K for most sources. It should be noted that the excitation temperature for L1551 is close to the rotational temperature of the carbon-chain molecules in L1527.

TABLE 4
Observed Positions

Sources	R.A. (J2000.0)	Decl. (J2000.0)	T_{ex}[a]	τ	N (10^{14} cm^{-2})
B1	03 33 16.34	+31 07 51.0	4.0(3)	0.28(2)	3.2(2)
L1489	04 04 50.60	+26 18 29.4	5.7(13)	0.06(3)	0.65(23)
L1498	04 10 51.46	+25 09 58.2	4.0(1)	0.54(17)	1.9(5)
L1495B	04 15 36.51	+28 47 05.9	4.3(f)	0.79(4)	3.2(1)
L1521B	04 24 12.67	+26 36 52.8	4.0(3)	0.36(23)	1.5(9)
L1521E	04 29 16.46	+26 13 49.6	4.4(2)	0.47(22)	2.2(10)
L1551	04 31 33.90	+18 08 05.1	9.4(32)	0.04(3)	1.6(4)
TMC-2	04 32 44.75	+24 24 33.5	4.3(1)	0.46(11)	2.2(5)
L1527[b]	04 39 53.59	+26 03 05.5	12.3(f)	0.14(2)	5.0(7)
TMC-1 (NH_3)	04 41 18.50	+25 48 13.6	4.2(1)	0.23(28)	1.8(6)
TMC-1 (CP)[b]	04 41 32.31	+26 00 42.7	6.7(f)	0.60(4)	6.7(5)
TMC-1C	04 41 42.49	+25 41 27.0	4.3(f)	0.72(5)	2.9(2)
L1544	05 04 15.25	+25 11 47.8	4.3(f)	0.48(16)	2.4(8)
L183	15 54 00.54	−02 51 48.5	4.3(f)	0.05(1)	0.19(3)
L1709B	16 31 39.63	−24 01 23.0	5.0(6)	0.20(9)	1.2(5)
ρ−Oph E[c]	16 32 29.45	−24 28 12.7	4.3(1)	0.18(2)	1.4(1)
L43	16 34 39.77	−15 46 43.5	4.4(4)	0.10(4)	0.92(25)
L63	16 50 15.53	−18 06 06.4	4.3(23)	0.20(6)	0.80(20)

Notes.—Numbers in parentheses represent the errors in units of the last significant digits. Units of right ascension are hours, minutes, and seconds, and units of declination are degrees, arcminutes, and arcseconds.

[a] The "f" means that the excitation temperature is fixed into the value given.

[b] These positions differ slightly (∼5″) from the position observed for other molecules in the 2005–2007 season.

[c] ∼1′ east of IRAS 16293−2422, which is the interaction region between the molecular outflow and the dense gas (Hirano & Taniguchi 2001).

REFERENCES

Aikawa, Y., Ohashi, N., Inutsuka, S., Herbst, E., & Takakuwa, S. 2001, ApJ, 552, 639
Aikawa, Y., Wakelam, V., Garrod, R. T., & Herbst, E. 2007, ApJ, in press (arXiv:0710.0712)
Alexander, A. J., Kroto, H. W., & Walton, D. R. M. 1976, J. Mol. Spectrosc., 62, 175
André, P., Ward Thompson, D., & Barsony, M. 2000, Protostars and Planets IV, ed. V. Mannings, A. P. Boss, & S. S. Russell (Tucson: Univ. Arizona Press), 59
Bell, M. B., Feldman, P. A., Travers, M. J., McCarthy, M. C., Gottlieb, C. A., & Thaddeus, P. 1997, ApJ, 483, L61
Benson, P. J., Caselli, P., & Myers, P. C. 1998, ApJ, 506, 743
Bottinelli, S., et al. 2004, ApJ, 615, 354
Burrell, P. M., Bjarnov, E., & Schwendeman, R. H. 1980, J. Mol. Spectrosc., 82, 193
Castets, A., et al. 2005, in ASP Conf. Ser. 344, The Cool Universe: Observing Cosmic Dawn, ed. C. Lidman, & D. Alloin (San Francisco: ASP), 212
Cazaux, S., Tielens, A. G. G. M., Ceccarelli, C., Castets, A., Wakelam, V., Caux, E., Parise, B., & Teyssier, D. 2003, ApJ, 593, L51
Cernicharo, J., Gottlieb, C. A., Guélin, M., Killian, T. C., Paubert, G., Thaddeus, P., & Vrtilek, J. M. 1991, ApJ, 368, L39
Cernicharo, J., Guélin, M., & Walmsley, C. M. 1987, A&A, 172, L5
Choi, M., Panis, J.-F., & Evans, N. J., II. 1999, ApJS, 122, 519
DeFrees, D. J., & McLean, A. D. 1986, ApJ, 308, L31
Guélin, M., Friberg, P., & Mezaoui, A. 1982, A&A, 109, 23
Hirano, N., & Taniguchi, Y. 2001, ApJ, 550, L219
Hirota, T., Ikeda, M., & Yamamoto, S. 2001, ApJ, 547, 814
Hirota, T., Yamamoto, S., Mikami, H., & Ohishi, M. 1998, ApJ, 503, 717
Hogerheijde, M. R., van Dishoeck, E. F., Blake, G. A., & van Langevelde, H. J. 1998, ApJ, 502, 315
Iida, M., Oshima, Y., & Endo, Y. 1991, ApJ, 371, L45
Irvine, W. M., Höglund, B., Friberg, P., Askne, J., & Elldér, J. 1981, ApJ, 248, L113
Kaifu, N., et al. 2004, PASJ, 56, 69
Kalenskii, S. V., Slysh, V. I., Goldsmith, P. F., & Johansson, L. E. B. 2004, ApJ, 610, 329
Kawaguchi, K., et al. 1991, PASJ, 43, 607
Killian, T. C., Vrtilek, J. M., Gottlieb, C. A., Gottlieb, E. W., & Thaddeus, P. 1990, ApJ, 365, L89
Kirby, C., Kroto, H. W., & Walton, D. R. M. 1980, J. Mol. Spectrosc., 83, 261
Langer, W. D., et al. 1997, ApJ, 480, L63
Maret, S., et al. 2004, A&A, 416, 577
Masunaga, H., & Inutsuka, S. 2000, ApJ, 531, 350
McCarthy, M. C., Chen, W., Apponi, A. J., Gottlieb, C. A., & Thaddeus, P. 1999, ApJ, 520, 158
Myers, P. C., Bachiller, R., Caselli, P., Fuller, G. A., Mardones, D., Tafalla, M., & Wilner, D. J. 1995, ApJ, 449, L65
Ohashi, N., Hayashi, M., Ho, P. T. P., & Momose, M. 1997, ApJ, 475, 211
Ohashi, N., Lee, S. W., Wilner, D. J., & Hayashi, M. 1999, ApJ, 518, L41
Pracna, P., Demaison, J., Wlodarczak, G., Lesarri, A., & Graner, G. 1996, J. Mol. Spectrosc., 177, 124
Sakai, N., Ikeda, M., Morita, M., Sakai, T., Takano, S., Osamura, Y., & Yamamoto, S. 2007c, ApJ, 663, 1174
Sakai, N., Sakai, T., Osamura, Y., & Yamamoto, S. 2007d, ApJ, 667, L65
Sakai, N., Sakai, T., & Yamamoto, S. 2006, PASJ, 58, L15
———. 2007a, ApJ, 660, 363
———. 2007b, Ap&SS, in press
Scappini, F., & Codella, C. 1996, MNRAS, 282, 587
Suzuki, H., Ohishi, M., Kaifi, N., Ishikawa, S., & Kasuga, T. 1986, PASJ, 38, 911
Suzuki, H., Yamamoto, S., Ohishi, M., Kaifu, N., Ishikawa, S., Hirahara, Y., & Takano, S. 1992, ApJ, 392, 551
Tafalla, M., Mardones, D., Myers, P. C., Caselli, P., Bachiller, R., & Benson, P. J. 1998, ApJ, 504, 900
Takakuwa, S., Mikami, H., Saito, M., & Naomi, H. 2000, ApJ, 542, 367
Takano, S., Suzuki, H., Ohishi, M., Ishikawa, S., Kaifu, N., Hirahara, Y., & Masuda, A. 1990, ApJ, 361, L15
Tamura, M., Ohashi, N., Hirano, N., Ito, Y., & Moriarty-Schieven, G. H. 1996, AJ, 112, 2076
Teyssier, D., Fossé, D., Gerin, M., Pety, J., Abergel, A., & Roueff, E. 2004, A&A, 417, 135
Thaddeus, P., Vrtilek, J. M., & Gottlieb, C. A. 1985, ApJ, 299, L63
Turner, B. E. 1989, ApJS, 70, 539
Turner, B. E., Herbst, E., & Terzieva, R. 2000, ApJS, 126, 427
Turner, B. E., Lee, H.-H., & Herbst, E. 1998, ApJS, 115, 91
van Dishoeck, E. F., Blake, G. A., Jansen, D. J., & Groesbeck, T. D. 1995, ApJ, 447, 760
Vrtilek, J. M., Gottlieb, C. A., & Gottlieb, E. W. 1990, ApJ, 364, L53
Wilson, S., & Green, S. 1977, ApJ, 212, L87
Winnewisser, G., Winnewisser, M., & Christiansen, J. J. 1982, A&A, 109, 141
Yamamoto, S., Saito, S., Kawaguchi, K., Chikada, Y., Suzuki, H., Kaifu, N., Ishikawa, S., & Ohishi, M. 1990, ApJ, 361, 318
Zhou, S., Evans, N. J., II, Wang, Y., Peng, R., & Lo, K. Y. 1994, ApJ, 433, 131